PRESSURE DISTRIBUTIONS ON THE VANES OF A RADIAL FLOW IMPELLER

by D. A. Morelli*

Summary

Theoretical approaches give very little guide to the design of radial arrays of vanes for the addition of energy to a fluid. The usual approach of the designer has been to design inlet and outlet angles according to the theory for an infinite number of vanes, and to connect these two angles by some plausible curve. Modifications are introduced according to the experience and records of the designer. The final justification of the design by measurements of the differential pressure is very rarely made.

The present paper reports the first of a series of planned experiments to develop necessary background knowledge. An impeller has been designed, according to stated assumptions, and the external characteristics, such as heads generated at various flow rates, have been measured in detail. These characteristics will be correlated with the distribution of the pressure on the vanes.

The paper will be illustrated by high-speed moving pictures of the flow in the relative and absolute coordinate systems.

Introduction

Radial flow rotors for handling liquids, such as the rotors of low specific speed pumps and turbines, have developed to a high efficiency with very little assistance from mathematics and mechanics. The excellent performance of these devices, under conditions of low system pressure where cavitation can occur, depends on the careful proportioning of inlet dimensions and vane curvatures to avoid areas of low pressure. Remarkable improvements have been achieved in pumps and turbines by intelligent interpretation of the results of tests of complete units. The record of progress is written in the current products of the manufacturing companies.

A research program would be of considerable value in developing, by the methods of fluid mechanics, a detailed knowledge of the action of the rotors of hydraulic machinery. Such a program is under way at the California Institute of Technology under the sponsorship of the Office of Naval Research.

Since a rotor of a pump impeller transfers mechanical energy to the fluid with an efficiency of the order of 95 per cent, it seems plausible that the flow conditions do not depart far from the potential flow of an incompressible fluid of vanishingly small kinematic viscosity. Earlier work (1), (2), (3)** reported studies of pump impellers operating in a polar symmetric collector using photographic techniques and examining in detail the total head generated by the rotating element. Reference (3) reported a technique

---

*Assistant Professor of Mechanical Engineering, Hydrodynamics Laboratories, California Institute of Technology.

**Numbers in parentheses refer to the bibliography at the end of the paper.

for measuring the losses incurred by the fluid passing through the rotor. All these techniques have led to better understanding of the action of the rotor but have shed little light on the distribution of the work on the rotor vanes or the origins of losses. It requires careful consideration and excellent physical insight to deduce accurately from such tests how an already good design should be improved.

Since, in potential flow, energy transfer occurs by the motion of the pressure forces on the moving boundaries, it is significant to examine in detail the distribution of pressure on the vanes of the rotating impeller. When cavitation susceptibility is being investigated, there is no substitute for this detailed knowledge of pressure distribution. Mathematical solutions of the problem would provide such information and can be readily formulated in general. However, they are enormously difficult to reduce to numerical results even in the simplest cases. Under these circumstances, the experimental approach of fluid mechanics can be used with advantage to interpret experimental results in a manner which extends their usefulness to a wider range of designs than that covered by the experimental tests.

Measuring Technique

Other experimenters have measured the pressures on the vanes of pump impellers, (4), but the techniques are mechanically complicated. The measurements were made by stationary manometers, and required multiple stuffing boxes or equivalent sliding seals for transfer of pressure from the rotating element.

In the Hydraulic Machinery Laboratory at the California Institute of Technology, it has been found practical to measure the characteristics of impellers at speeds below 400 rpm on impellers up to 13 in. in size. The scale effect was investigated in earlier work and does not appear to be significant. At these low speeds a multiple tube manometer can be mounted directly on the pump impeller, and the vertical overhung type of pump drive used in these tests permits the use of a tubular manometer mounting carefully centered around the axis of rotation. In the installation illustrated in Fig. 1, there are thirty tubes of uniform diameter connected at the top by a manifold ring. These are held closely against the tubular mounting and can be connected by small bore tygon tubing to any thirty of the one hundred pressure taps on the impeller. All connecting tubes to the pressure taps are filled with the water which was the working fluid of these tests. The tubular mount is graduated axially in hundredths of a foot, and readings are made by a strobolux light actuated by a contactor.

The pressures are measured as differentials by a procedure which keeps the differentials within the limits of the graduated range of the manometer. The ungraduated extension of the tubes, visible in Fig. 1, is a precaution against overshoot and simplifies operation. All pressures are referred to the total head at the center line of the inlet pipe as zero. The reference pressure tap is connected by a hole through the hub to a total-head tube on the center line of the inlet pipe. When a hole at which the pressure is p, is connected through the rotating differential manometer to the total-head tube at the center of rotation where the pressure is p_T, the differential head, ΔH, read on the manometer is given by

$$\frac{u^2}{2g} - \Delta H = \frac{p - p_T}{\rho g} \qquad (1)$$

The general description of the auxiliary facilities of the Laboratory is given in previous publications (1),(2),(3), and will not be discussed here. Material reported in (3) will be used in later sections of this paper to illustrate the relation between pressure distribution and performance. The references to (3) are brief and the interested reader should seek the detail in the original paper.

Test Impeller

An axial cross section of the impeller used for this work is shown in Fig. 2. The vanes extend from radius 3.0 in. to radius 5.15 in. between parallel shrouds with an unconventional approach. The unusual shroud profiles were chosen in an effort to achieve symmetry at the inlet edge and have proved relatively successful. They can be improved further by increasing the inlet radii. The six vanes were made from 0.093 in. sheet stock set in flutes milled to template and accurately spaced at 60° intervals. Inlet and outlet tips are rounded to the thickness of the material.

Figure 3 is a view of the impeller fitted with pressure connections. The pressure taps are 0.030 in. holes connected to 1/16 in. brass tubes which pass up through clearance holes in the top shroud. In each vane there are sixteen pressure measuring stations arranged at three levels and distributed over the concave and convex sides of the vane. Each of the six vanes has a particular distribution of pressure taps, as shown in the pressure tap location diagram inserted as Fig. 4. Under conditions of symmetrical flow, the data from all pressure taps can be considered as applying to one vane, while for asymmetrical flow each vane must be considered separately. The impeller was run at 225 rpm and satisfies the general dimensions of Fig. 2. The vane shape constants were

$$K_1 = 1.724 \qquad \frac{r_1}{r_2} = 0.58 \qquad \beta_2 = 23.5^\circ \qquad \frac{c_{m2}}{u_2} = 0.12$$

These quantities, when introduced into Eq. (4), give the vane shape equation

$$\phi = 8.30 \frac{r}{r_2} - 3.00 \left(\frac{r}{r_2}\right)^2 \qquad (2)$$

where ϕ is measured from $\frac{r}{r_2} = 0$.

Impeller Design

Vane curvature is arbitrarily defined by postulating an infinite number of vanes and a linear increase of the tangential component, c_u, of the absolute velocity of the fluid as it passes through the passages. The outlet angle, β_2, at the vane tips, measured from the tangent, is arbitrarily chosen as 23.5°, and determines the rate of increase of c_u.

The differential equation for the vane in polar coordinates is

$$\frac{dr}{r\,d\phi} = \frac{c_m}{u\left(1 - \frac{c_u}{u}\right)} \tag{3}$$

Assuming a linear growth of c_u from zero as r increases from r_1, then

$$c_u = K_1 \omega (r - r_1)$$

and, for uniform flow across a two-dimensional impeller,

$$c_m = \frac{r_2 c_{m2}}{r}$$

where the subscripts 1 and 2 refer to inlet and outlet, respectively.

The differential equation (3) becomes

$$\frac{d\phi}{dr} = \frac{\omega}{r_2 c_{m2}} \left[(1 - K_1) r + K_1 r_1 \right]$$

The solution for this equation gives the vane equation

$$\phi = \frac{u_2}{c_{m2}} \left[\frac{r^2}{2 r_2^2} (1 - K_1) + K_1 \frac{r_1 r}{r_2^2} \right] \tag{4}$$

If the relative flow at the outlet is determined by β_2, the vane outlet angle, then

$$K_1 = \frac{1 - \frac{c_{m2}}{u_2} \cot \beta_2}{1 - \frac{r_1}{r_2}} \tag{5}$$

At flow rate $(c_{m2}/u_2)'$, other than the design flow rate c_{m2}/u_2, the tangential component becomes

$$\left(\frac{c_u}{u_2}\right)' = \left[1 - \left(\frac{c_{m2}}{u_2}\right)' \cdot \frac{u_2}{c_{m2}} \right] \frac{u}{u_2} + \left(\frac{c_{m2}}{u_2}\right)' \cdot \frac{u_2}{c_{m2}} \cdot \frac{c_u}{u_2} \tag{6}$$

Equation (6) shows that the vane shape given by Eq. (4) gives a linear growth of c_u at all flow rates. At flow rates other than the design flow rate there is a singularity in the distribution of c_u at the inlet.

The circulation around the impeller axis at radius r is given by

$$\Gamma = 2\pi r \left(\frac{c_u}{u_2}\right)' \cdot u_2$$

$$= \left[1 - \left(\frac{c_{m2}}{u_2}\right)' \cdot \frac{u_2}{c_{m2}} \right] 2\pi r u + \left(\frac{c_{m2}}{u_2}\right)' \cdot \frac{u_2}{c_{m2}} \cdot 2\pi K_1 u (r - r_1)$$

and

$$\frac{d\Gamma}{dr} = \left[1 - \left(\frac{c_{m2}}{u_2}\right)' \frac{u_2}{c_{m2}}\right] 4\pi u + \left(\frac{c_{m2}}{u_2}\right)' \cdot \frac{u_2}{c_{m2}} \left(2 - \frac{r}{r}\right) 2\pi K_1 u$$

$$= \frac{d\Gamma}{ds \sin\beta} \tag{7}$$

When comparing with the circulation distribution for a finite number of vanes, Eq. (7) must be divided by the number of vanes

$$\left(\frac{d\Gamma}{dr}\right)_z = \frac{1}{z} \cdot \frac{d\Gamma}{dr} = \frac{1}{z} \cdot \frac{d\Gamma}{ds \sin\beta} \tag{8}$$

The Meaning of Pressure Measurements

By writing the Bernoulli relation for steady flow of a nonviscous incompressible fluid for a coordinate system rotating about a fixed origin at angular velocity ω , one obtains the statement of pressure in terms of relative velocities and the motion of the coordinate axes. For convenience it is written here in terms of head instead of pressure.

$$H_a + \frac{w^2}{2g} - \frac{\omega^2 r^2}{2g} = \text{constant}$$

The choice of total head, H_T, at the axis of rotation as datum of measurement, yields

$$H_a - H_T = H = \frac{\omega^2 r^2}{2g} - \frac{w^2}{2g} = \frac{u^2}{2g} - \frac{w^2}{2g} \tag{9}$$

By equating Eqs. (1) and (9) it is seen that

$$\Delta H = \frac{w^2}{2g} \tag{10}$$

Equation (10) permits calculation of the magnitude of the relative velocities from the pressure measurements.

For two points on opposite faces of a vane at the same radius, and using the subscripts p and s to denote pressure face and suction face, respectively, we obtain

$$\frac{\Delta p}{\rho g} = \Delta H_s - \Delta H_p = \frac{w_s^2 - w_p^2}{2g}$$

$$= \frac{2}{g} \cdot \frac{w_s + w_p}{2} \cdot \frac{w_s - w_p}{2}$$

$$= \frac{2}{g} \cdot w_{av.} \cdot w_{diff.}$$

$$\Delta p \, ds = 2\rho \, w_{av.} \cdot w_{diff.} \cdot ds = \rho \, w_{av.} \, d\Gamma$$

and

$$\Delta p \cdot dr = \rho \sin\beta \cdot w_{av.} \cdot d\Gamma$$

The torque on Z vanes of width b is then

$$T = b \cdot z \int_0^{r_2} \Delta p \cdot r \cdot dr = \rho b z \int_0^{r_2} w_{av.} \, r \cdot \sin\beta \left(\frac{dr}{dr}\right)_z \cdot dr$$

From general theorems of hydrodynamics, the torque

$$T = b z \int_0^{r_2} \Delta p \cdot r \, dr = \rho b r_2 \, c_{m2} \cdot \Gamma$$

w_{av} can be expressed as a product of the meridional velocity and a function F of the vane shape

$$w_{av.} = F \cdot \frac{c_m}{\sin\beta} = F \cdot \frac{c_{m2}}{\sin\beta} \cdot \frac{r_2}{r} = F \cdot w_{calc.}$$

It should be noted that the foregoing deductions are based on perfect fluid flow which involves no losses. Therefore the equations cannot be considered precise in any case, although in the regions of operation where the flow suffers no large velocity changes or separation, they are not greatly in error.

Experimental Results

Figures 5(a) to 5(n)* show the static pressure plotted in dimensionless form against the radius ratio as abscissa, for various flow rates defined by the values of c_{m2}/u_2. The experimental points are shown individually to illustrate the variation which occurs over the width of the impeller. The legend should be interpreted in conjunction with Fig. 4. The figures also contain the forced vortex reference line which is the base line for measurement of Δ H in Eq. (10). Static pressures are measured above inlet total head, therefore the pressures at some point near the inlet edge of the vane must fall below the abscissa axis by at least the inlet velocity head.

The most significant deviations from two-dimensional conditions will be observed near the inlet edge of the vane. As the flow rate varies, the asymmetry at the inlet edge changes in character. The high and low pressures interchange places as the flow rate increases.

At flow rates smaller than 0.11 the pressure diagram shows a large local underpressure over large areas at the inlet edge on the concave side of the vane. At slightly greater flow rates, the underpressure disappears. When the high-speed motion pictures of the flow are studied in detail, it will be seen that the flow is very turbulent along the concave side below the critical flow rate. There is, however, no evidence of separation until the flow rate has

---

*Parts of Fig. 5 and Fig. 8 have been deleted from the paper in order to reduce its length.

been decreased well below the 0.11.

Separation on the concave side becomes evident in the pressure diagrams and the flow pictures at flow rates below 0.061, and leads to the characteristic asymmetrical flow in alternate passages, which is evident in the pressure distribution shown in Figs. 5(b) to 5(c). In these figures the data from all pressure taps cannot be applied to one vane but cognizance must be taken of the particular passage in which the pressure tap lies. The diagram then shows two pressure loops which illustrate the asymmetry prevailing in alternate passages.

At shut-off, Fig. 5(a), the asymmetry disappears almost entirely and the pressure diagram defines a flow pattern consisting of forced vortex flow in the inner part of the passage, and an eddy in the outer part. The location of the pressure diagram with respect to the forced vortex reference line shows that there is very little pre-rotation in the inlet to the impeller.

These observations have been well substantiated by visual studies with motion pictures, but it is difficult to detect close detail on visual studies. The inherent value of pressure studies lies in its ability to show the fine points which give rise to important over-all effects.

Influence of Relative Inlet Angle

If one disregards the local asymmetries in the pressure distributions in the neighborhood of the inlet, the trend of the vane pressure data as the flow rate is increased can be correlated with the head-capacity curve of Fig. 6. For convenience, the flow rates defined in Fig. 5 are marked in Fig. 6 with their proper figure numbers. At shut-off there is very little relative motion between fluid and vane, and no severe underpressures exist at the inlet. For this impeller, the flow conditions between shut-off and a flow rate of about 0.06 are asymmetrical and there is separation on the concave side in alternate passages. The underpressures are suppressed by the separation. Stated in another way, alternate vanes are stalled. As flow rates increase, the separation disappears and adverse entrance angles are indicated by the severe underpressures which appear on the concave side at the inlet edge. The range of flow between 0.06 and 0.11 could be classified as a zone of high cavitation susceptibility.

Flow rates which show a pronounced region of underpressure on the concave side of the vane are interesting in another way. At the low flow end of this range, where the pattern of flow changes from symmetrical to asymmetrical, the discontinuity in the head-capacity curve appears. This is evident in Fig. 6 and Fig. 7. The latter figure was taken from a previous publication,(3), and it shows also the effect of the location of the total-head tube on the measurements of total head. It will be seen that there are differences between the measurements at a point 1/16 in. from the periphery of the impeller and those obtained at a greater distance from the periphery. The origin of this discrepancy is seen in the pressure diagrams, Fig. 5. The point of divergence of the two curves of Fig. 7 coincide with the highest flow rate at which a significant area of negative pressure occurs on the concave side of the vanes, as illustrated by Fig. 5(g).

Between flow rates of 0.11 and 0.151, there are no severe local underpressures but the negative part of the pressure loop is getting generally

lower, showing an increasing cavitation susceptibility. At 0.151 the entrance angle again becomes unsatisfactory, but on the pressure side. At this point the incipient stall on the pressure side of the vane is apparent in Fig. 6, which shows a pronounced bend in curve A. As the flow rate increases still further, the adverse entrance angle results in large underpressures at the inlet edge on the pressure side, and general separation on the pressure side is visible in the flow motion pictures. In Fig. 6, curve C develops a bend which also indicates a stalled condition. The underpressures at very high flow rates near zero head become larger numerically than the maximum positive pressures elsewhere on the vanes. The experimental data for these flow rates have not been included in this paper.

The two zones of high cavitation susceptibility demonstrated by Gongwer (5), from studies of complete pumps, are fully substantiated and can be attributed almost wholly to unsatisfactory inlet angles.

It was assumed in the beginning of this section that underpressures which did not extend over appreciable areas were not of very great importance in the performance of the impeller. The elimination of such localized low pressures requires extreme attention to detail and ideal approach velocities, conditions which cannot be achieved in practice. However, in the over-all picture, there is a zone of operation which is much better than any other and its location depends principally on the configuration of the inlet. Within the channel proper, it appears that a smoothly contoured vane will give very good pressure distributions regardless of what occurs at the inlet.

Relative Velocities

If one accepts the postulate that, in the range of high efficiency, the flow pattern through the impeller departs little from potential flow, it is possible to calculate the relative velocities of the potential flow at the vane surfaces from the pressure measurements. For the impeller on which the present paper is based, the range of operation for which calculations can be made with assurance is between flow rates of 0.11 and 0.140. All velocities have been calculated as dimensionless ratios based on the peripheral speed u_2. The subscripts s and p define the suction and pressure sides of the vane, respectively. The quantities calculated and plotted in Figs. 8(a) to 8(d) are the dimensionless relative velocities W_p and W_s, the average dimensionless velocity, and one-half of the difference between the dimensionless velocities.

$$W_{av.} = \frac{W_s + W_p}{2} \quad , \quad W_{diff.} = \frac{W_s - W_p}{2}$$

Two other quantities are interesting, viz., the ratio of the dimensionless relative velocities W_p/W_s, and the dimensionless relative velocity calculated from the impeller dimensions and the flow rate W_{calc}. This is essentially the assumption of an infinite number of infinitely thin vanes.

Comparing the values of W_{av} and W_{calc} in any one of Figs. 8(a) to 8(d), it will be seen that the velocity calculated on the basis of an infinite number of vanes is not an acceptable approximation of the relative velocity. The very large divergence between the two values at the outlet tip accounts for the difference between the head generated by a finite number of vanes and that

calculated on the basis of Euler's infinite vane theory. The concept of a flow deviation or "slip" at the tip is not necessary for the explanation of this deficiency in head generated. The Kutta condition at the outlet tip is satisfied by an increased relative velocity above that calculated from uniform meridional outflow around the periphery of the impeller. That the Kutta condition is closely satisfied in these cases has been well established by visual examination of the flow. Considerations of continuity require, then, that the meridional velocity be less in midpassage than at the venes, a condition which has been proved both experimentally and theoretically.

The curves of W_{diff} define the distribution of circulation $d\Gamma/dr$ and are of theoretical interest to the designer, since the basic theoretical problem of potential theory is intimately related to the generation and distribution of circulation. Further discussion of this topic is not the province of this paper.

It is obvious from continuity that the average velocity should increase with increasing flow rate. It is only slightly less obvious that the maximum and minimum velocities should both increase with increasing flow rate. These points are exemplified by the plots of dimensionless maximum and minimum velocities in Figs. 8(a) to 8(d). The ratio of these two velocities is quite large for heavily loaded vanes. It is conceivable, and borne out theoretically, that loading can be increased by reducing the number of vanes or increasing the vane angle, to such an extent that the minimum velocity becomes zero at some point on the pressure side of the vane. At higher loading the minimum velocity becomes negative. Reverting to Eq. (9), this is tantamount to saying that the maximum pressure which can be achieved on the vanes is the forced vortex pressure defined by the forced vortex reference line shown in Figs. 5(a) to 5(n). There is, however, no such theoretical limit on the low pressure side except that imposed by cavitation limits. The cavitation limits can be removed by increasing the system pressure.

Aside from increasing loading by changing the vane angle or the number of vanes, it is possible to reach the condition at which back-flows occur in the impeller in another way. If one attempts to design an impeller of given vane angle to operate at very low values of c_{m2}/u_2, the following state of affairs arises. Because of the low through-flow velocity, the relative velocity along the vane is low, as indicated previously. At the same time the difference in relative velocities on the two sides of the vane increases, because, with backward curved vanes, the theoretical head increases with decreasing flow rate. To clarify this statement further, it is noted that circulation is directly proportional to the head generated. In attempting to design for low flow rates and high head, that flow pattern can again be reached which results in reversed velocity on the pressure side of the vane. It will be seen from the nature of the water horsepower characteristic that the vanes of such a pump are comparatively lightly loaded.

Potential backflows within the impeller cannot be conducive to high efficiency and the ratio of maximum to minimum velocity must be considered as a design parameter.

Cavitation Parameters

The Figs. 5(a) to 5(n) show dimensionless head measured from the total head at the inlet as datum. Where the pressure loop falls below the datum line, pressures occur on the vanes which are lower than the inlet total head. If the inlet total head at any time is reduced to such a value that the absolute pressure at the region of lowest pressure passes below the vapor pressure of the working fluid, then boiling (cavitation) may occur in that region. The Figs. 5(a) to 5(n) can supply in dimensionless form the net positive suction head (NPSH) for operation without cavitation on the vanes. Those familiar with the literature on the subject (6),(7), can deduce therefrom the common parameters of cavitation quality such as Thoma's Sigma (σ) and Suction Specific Speed (n_s) for special cases.

Conclusion

This paper has been written to exemplify the technique and applicability of pressure measurements at a great number of points along the impeller vanes, and gives a brief survey of how the data obtained may be used. It concludes with the hope that similar measurements, with impellers modified step by step, will separate the effects of every change and lead to a better understanding of the details of design which were heretofore studied only in their overall performance.

Bibliography

1. Osborne, W. C. and Morelli, D. A., "Head and Flow Observations on a High Efficiency Centrifugal Pump Impeller," Trans. ASME, Vol. 72, 1950, pp. 999-1006.

2. _____, "Measured Performance of Pump Impellers," Preprint No. 50-A-90, presented at Annual Meeting ASME, Nov. 26-Dec. 1.

3. Beveridge, J. H., and Morelli, D. A., "Evaluation of a Two-Dimensional Centrifugal Pump Impeller," Preprint No. 50-A-147, ASME.

4. Hagmayer, Erich, "Messungen des Druckverlaufes über Lauf. - und Leitschaufel einer Kreiselpumpe Innerhalb und Auszerhalb des Gebietes der Kavitation," Dissertation - Braunschweig 1932.

5. Gongwer, C., "A Theory of Cavitation Flow in Centrifugal Pump Impellers," Trans. ASME, Vol. 63, No. 1, Jan. 1941.

6. Stepanoff, A. J., "Centrifugal and Axial Flow Pumps, John Wiley and Sons, Inc., New York, 1948.

7. Wislicenus, G. F., "Fluid Mechanics of Turbomachinery," McGraw-Hill Co., New York, 1948.

Nomenclature

b = width of vane

β = vane angle measured from tangent

c_m = meridional velocity of fluid

c_u = tangential component of absolute velocity of fluid

ϕ = angular coordinate about center of impeller

g = acceleration due to gravity

Γ = total circulation around the axes of rotation

H = static head above inlet total head

H_a = $p/\rho g$ = static head at a pressure tap

H_T = total head at centerline of inlet pipe

ΔH = differential head read on manometer

h = head generated by impeller

K_1 = impeller design constant

p = pressure at a pressure tap

p_T = total pressure at centerline of inlet pipe

r = radial coordinate from center of impeller

s = distance along vane

u = ωr = tangential velocity of impeller at radius r

w = relative velocity

W = dimensionless relative velocity

ω = angular velocity of impeller

z = number of vanes

Figure Captions

Fig. 1 - Impeller and rotation manometer installed in the test basin.
Fig. 2 - Axial cross section of the impeller.
Fig. 3 - Assembled view of the test impeller.
Fig. 4 - Drilling diagram for pressure taps.
Fig. 5 - Static head on vanes at various flow rates.
Fig. 6 - Unit head vs. unit capacity at three locations across the outlet width.
Fig. 7 - Effect of radial distance of total-head tube on measured head.
Fig. 8 - Dimensionless velocities at various flow rates.

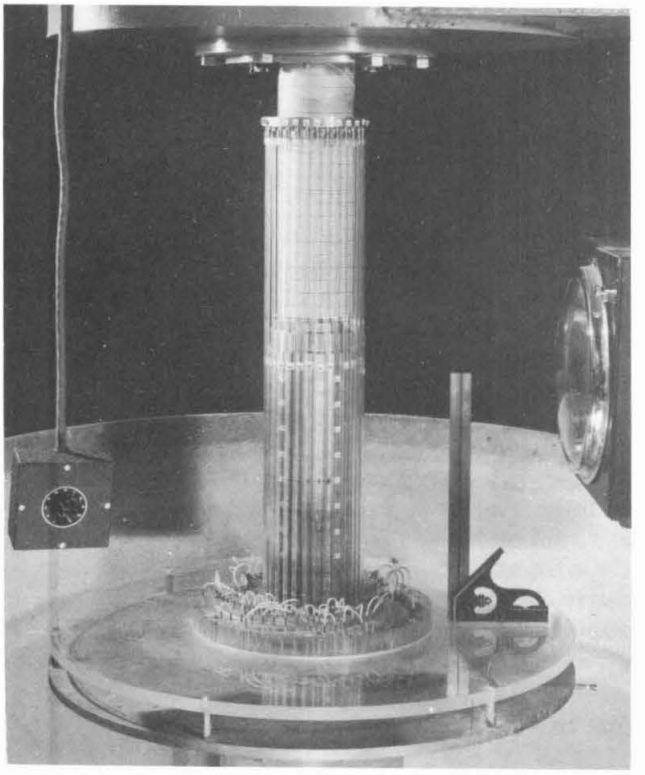

Fig. 1 - Impeller and rotating manometer installed in the test basin.

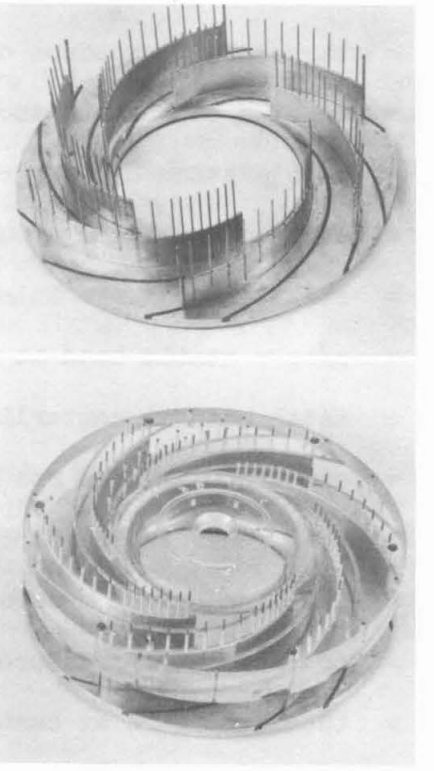

Fig. 3 - Bottom shroud with vanes and assembled view of test impeller.

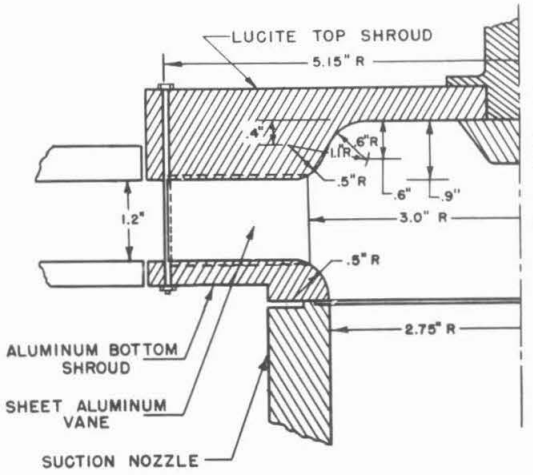

Fig. 2 - Axial cross section of the impeller.

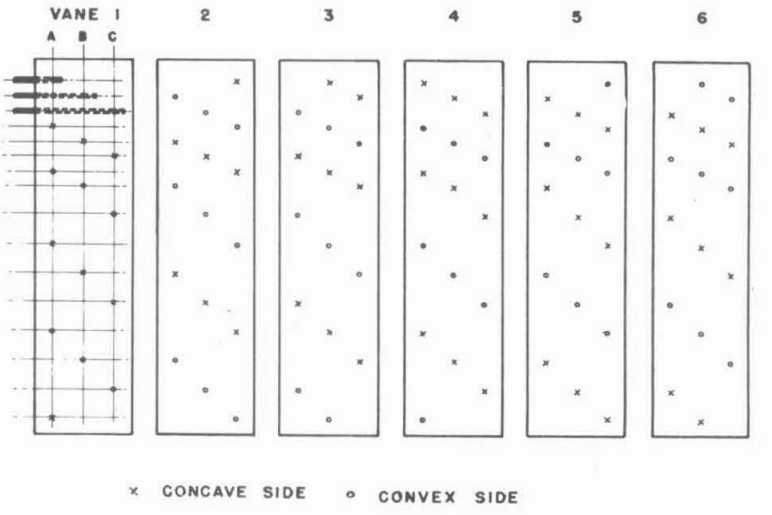

Fig. 4 - Drilling diagram for pressure taps.

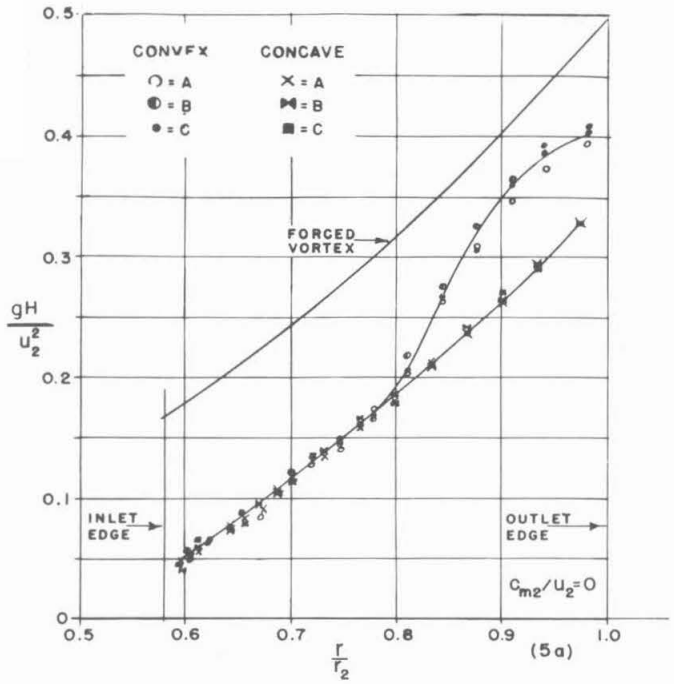
CONVEX
CONCAVE
○ = A
◐ = B
● = C
× = A
⋈ = B
■ = C
FORCED VORTEX
INLET EDGE
OUTLET EDGE
$C_{m2}/u_2 = 0$
$\frac{gH}{u_2^2}$
$\frac{r}{r_2}$
(5a)

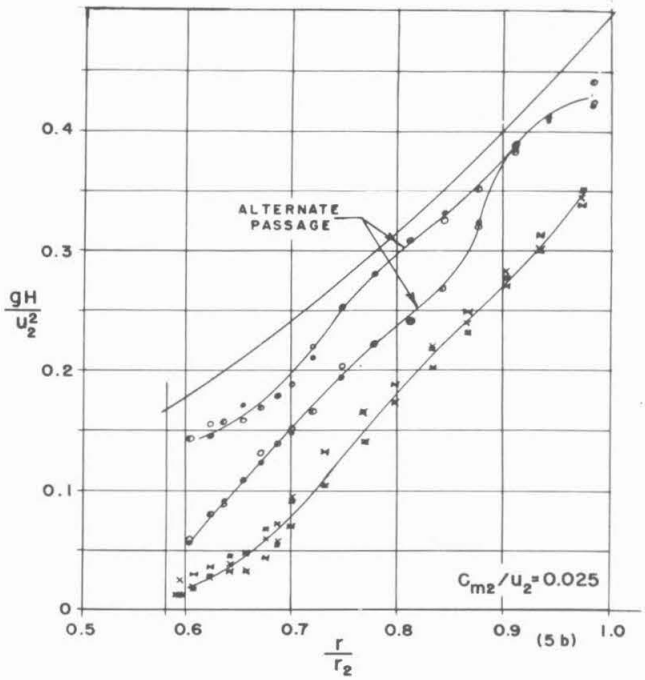
ALTERNATE PASSAGE
$C_{m2}/u_2 = 0.025$
$\frac{gH}{u_2^2}$
$\frac{r}{r_2}$
(5b)

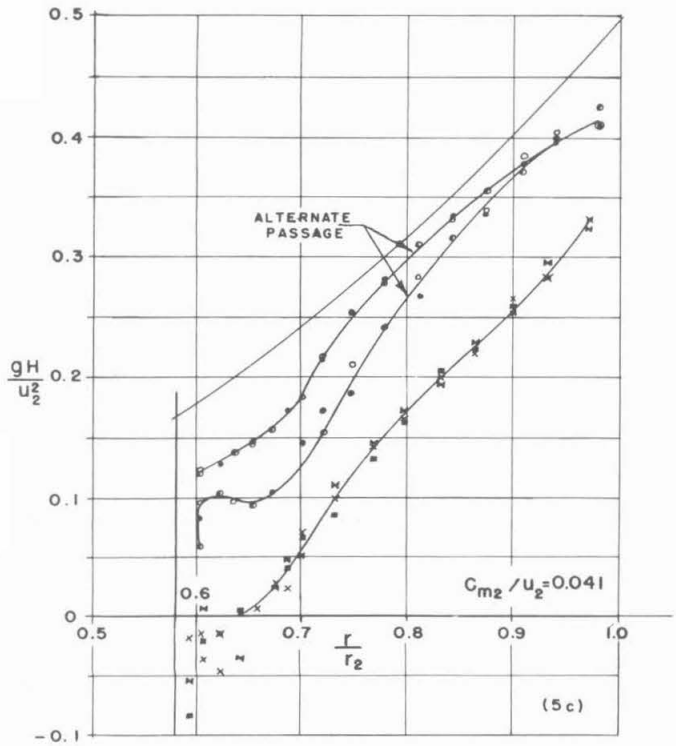
ALTERNATE PASSAGE
$C_{m2}/u_2 = 0.041$
$\frac{gH}{u_2^2}$
$\frac{r}{r_2}$
(5c)

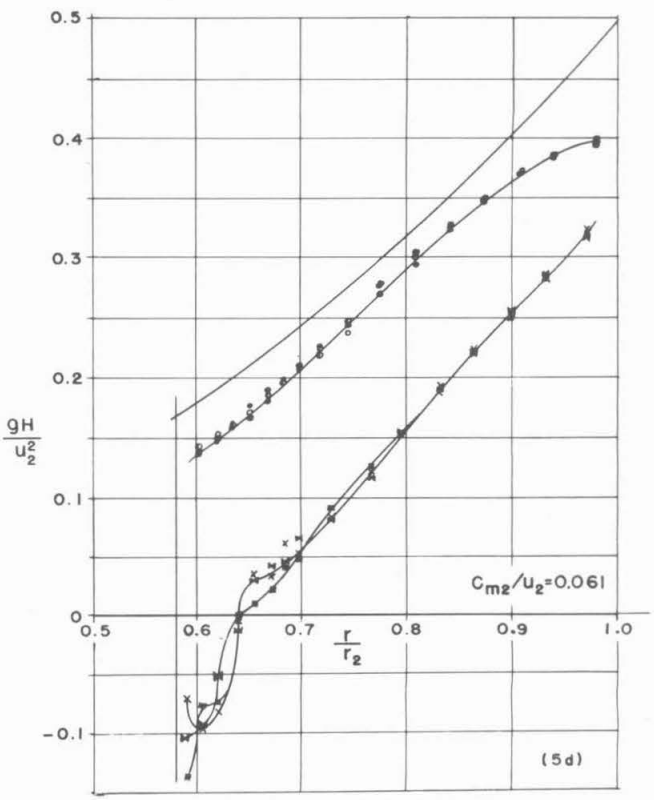
$C_{m2}/u_2 = 0.061$
$\frac{gH}{u_2^2}$
$\frac{r}{r_2}$
(5d)

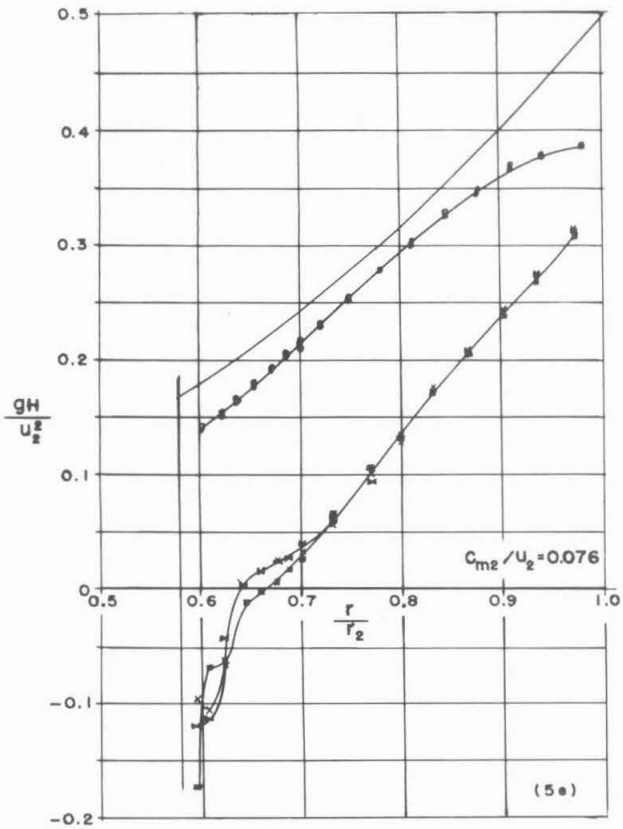
0.5
0.4
0.3
0.2
0.1
0
-0.1
-0.2
gH/u₂²
0.5
0.6
0.7
0.8
0.9
1.0
r/r₂
Cm2/u2=0.076
(5e)

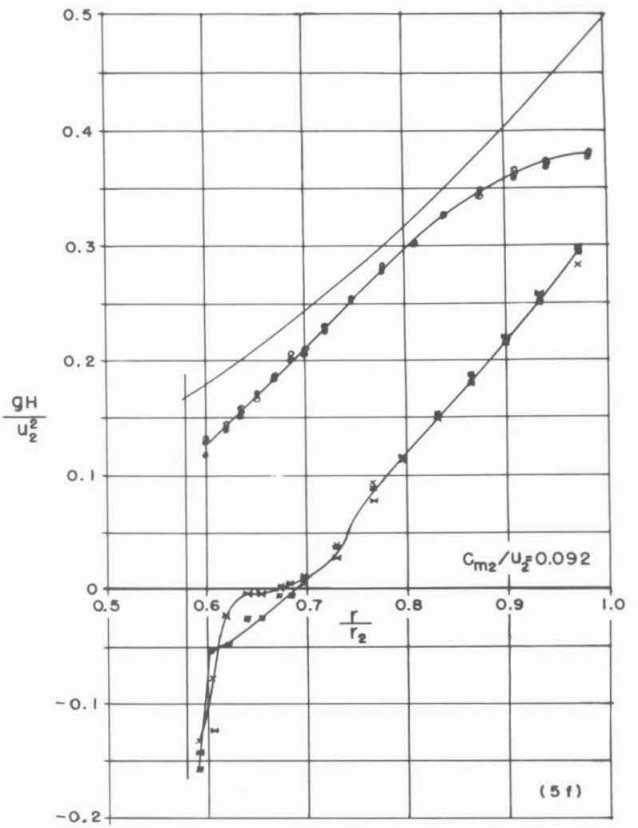
0.5
0.4
0.3
0.2
0.1
0
-0.1
-0.2
gH/u₂²
0.5
0.6
0.7
0.8
0.9
1.0
r/r₂
Cm2/u2=0.092
(5f)

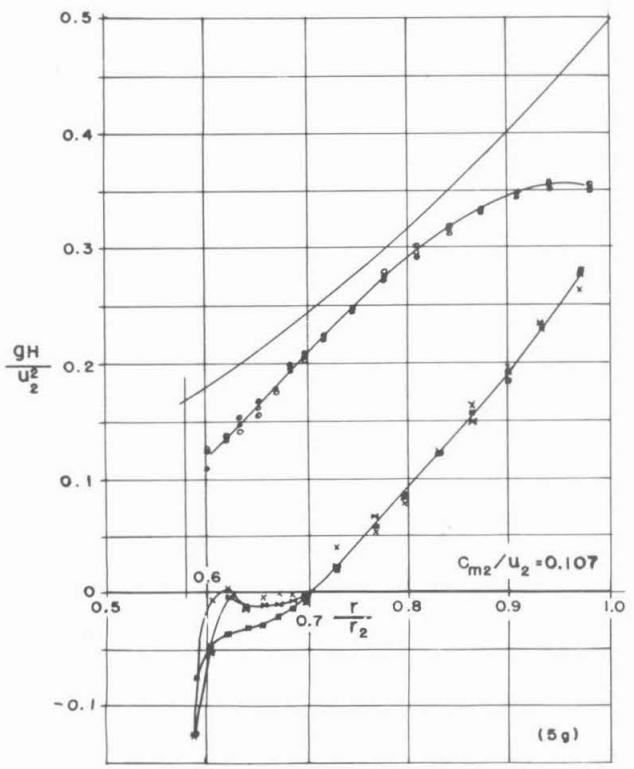
0.5
0.4
0.3
0.2
0.1
0
-0.1
gH/u₂²
0.6
0.5
0.7
0.8
0.9
1.0
r/r₂
Cm2/u2=0.107
(5g)

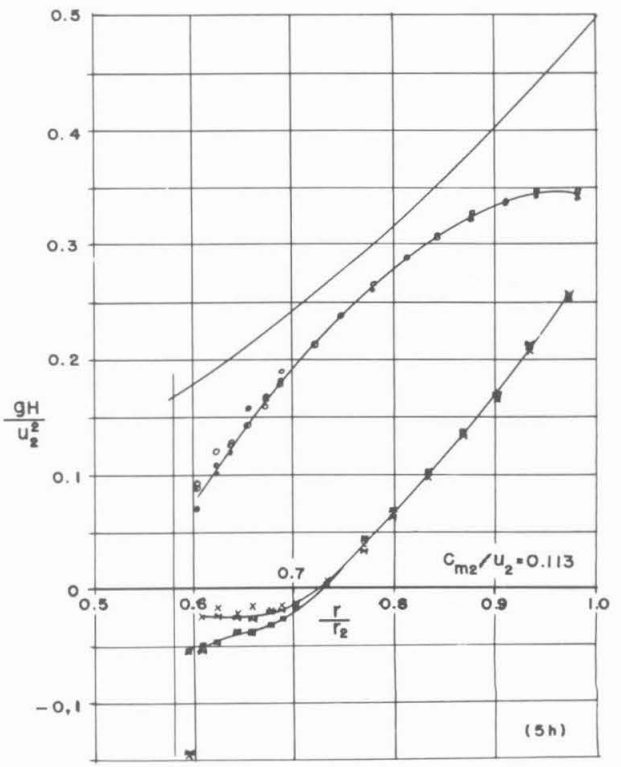
0.5
0.4
0.3
0.2
0.1
0
-0,1
gH/u₂²
0.7
0.6
0.5
0.8
0.9
1.0
r/r₂
Cm2/u2=0.113
(5h)

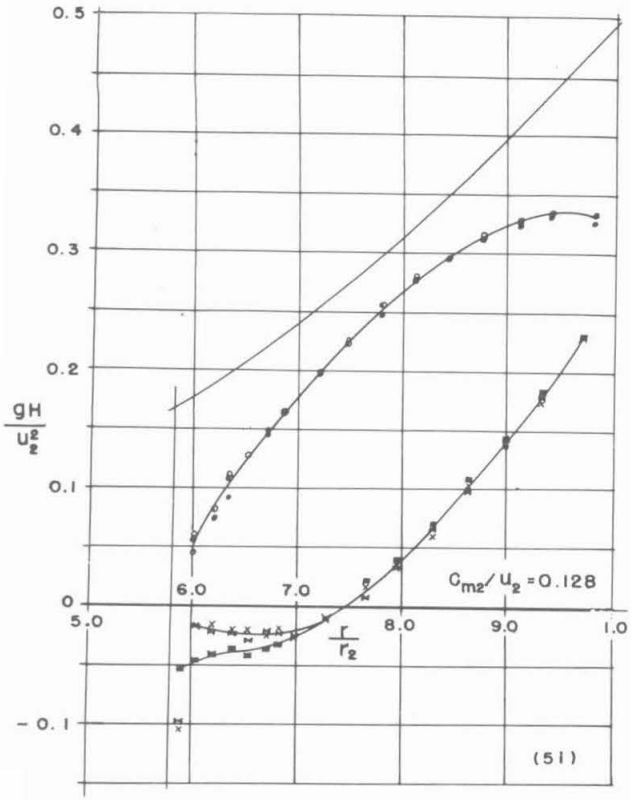
0.5
0.4
0.3
0.2
0.1
0
-0.1
gH/u2²
5.0
6.0
7.0
8.0
9.0
1.0
r/r2
Cm2/u2 = 0.128
(5 i)

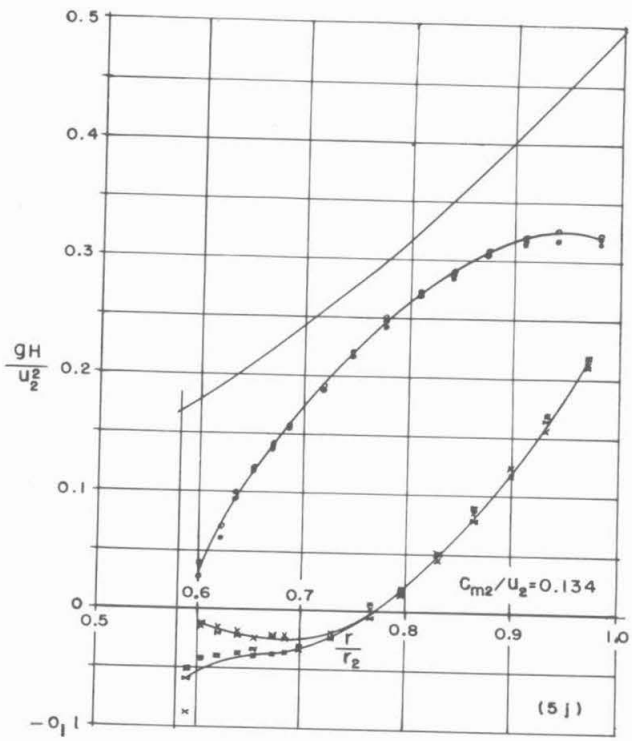
0.5
0.4
0.3
0.2
0.1
0
-0.1
gH/u2²
0.5
0.6
0.7
0.8
0.9
1.0
r/r2
Cm2/u2 = 0.134
(5 j)

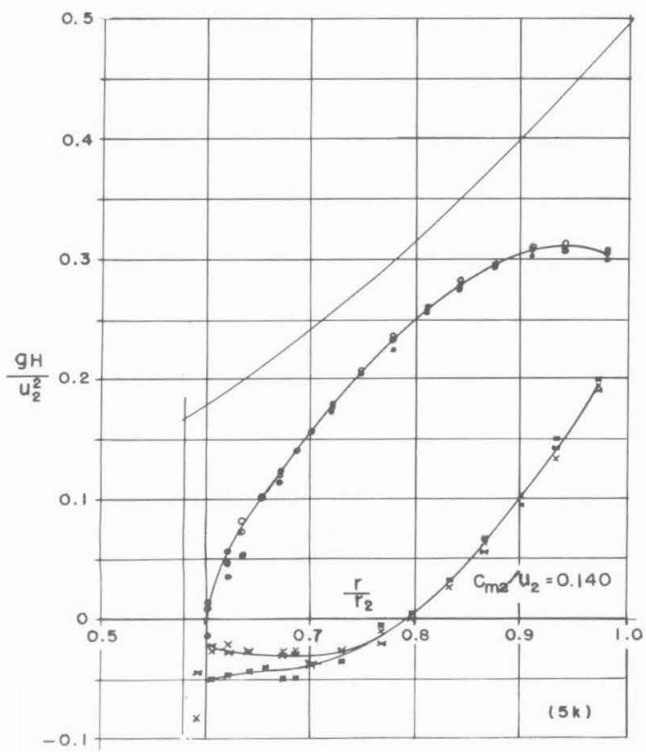
0.5
0.4
0.3
0.2
0.1
0
-0.1
gH/u2²
0.5
0.7
0.8
0.9
1.0
r/r2
Cm2/u2 = 0.140
(5 k)

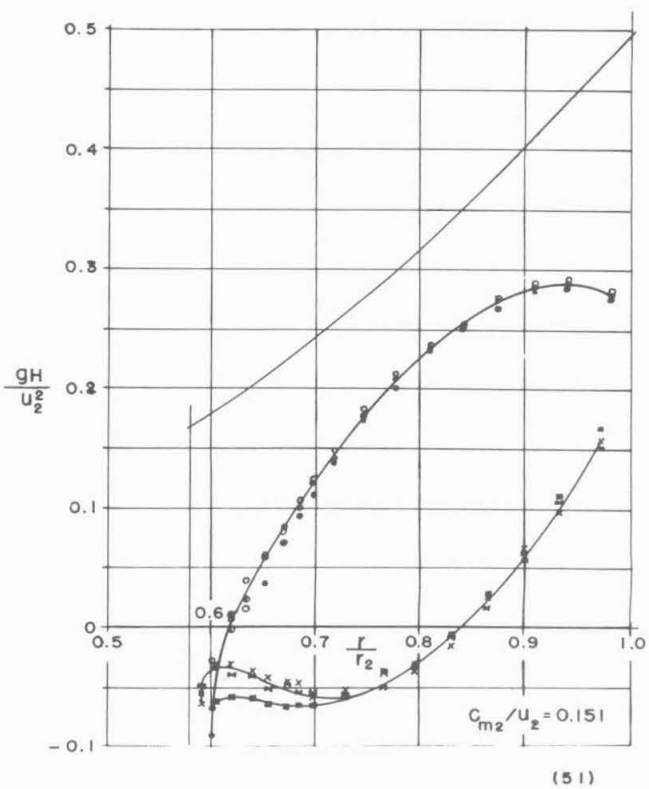
0.5
0.4
0.3
0.2
0.1
0
-0.1
gH/u2²
0.6
0.5
0.7
0.8
0.9
1.0
r/r2
Cm2/u2 = 0.151
(5 l)

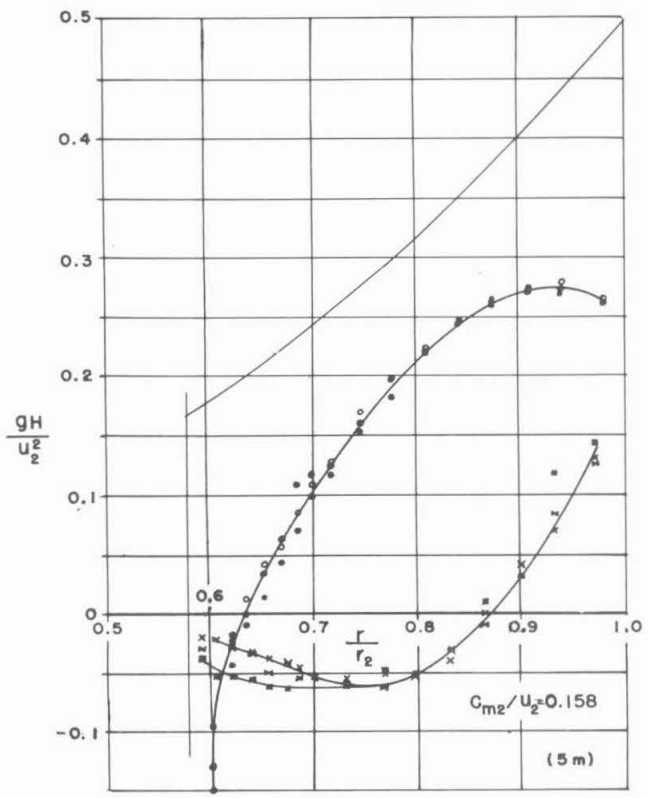
0.5
0.4
0.3
0.2
0.1
0
-0.1
gH/u2²
0.6
0.5
0.7
0.8
0.9
1.0
r/r2
Cm2/u2=0.158
(5m)

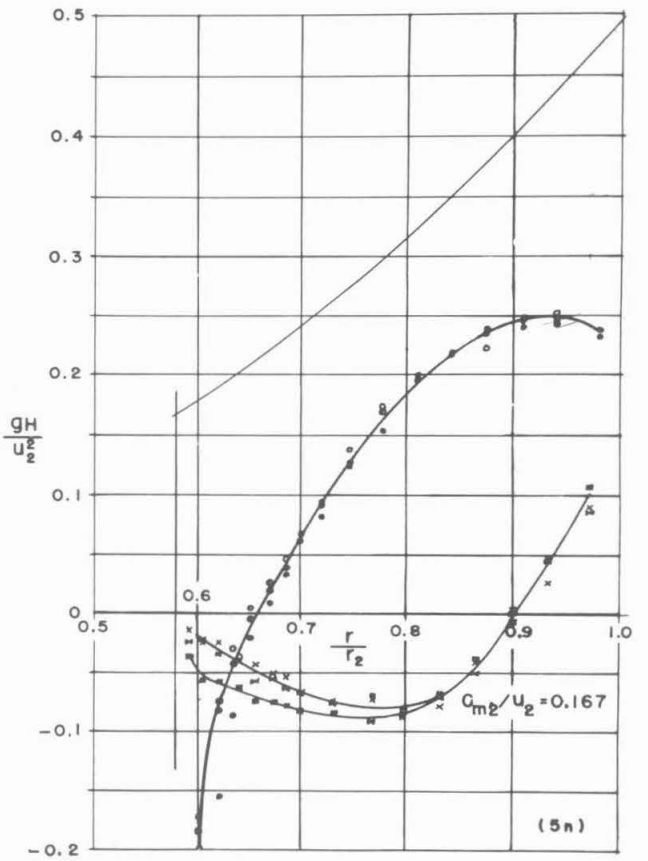
0.5
0.4
0.3
0.2
0.1
0
-0.1
-0.2
gH/u2²
0.6
0.5
0.7
0.8
0.9
1.0
r/r2
Cm2/u2=0.167
(5n)

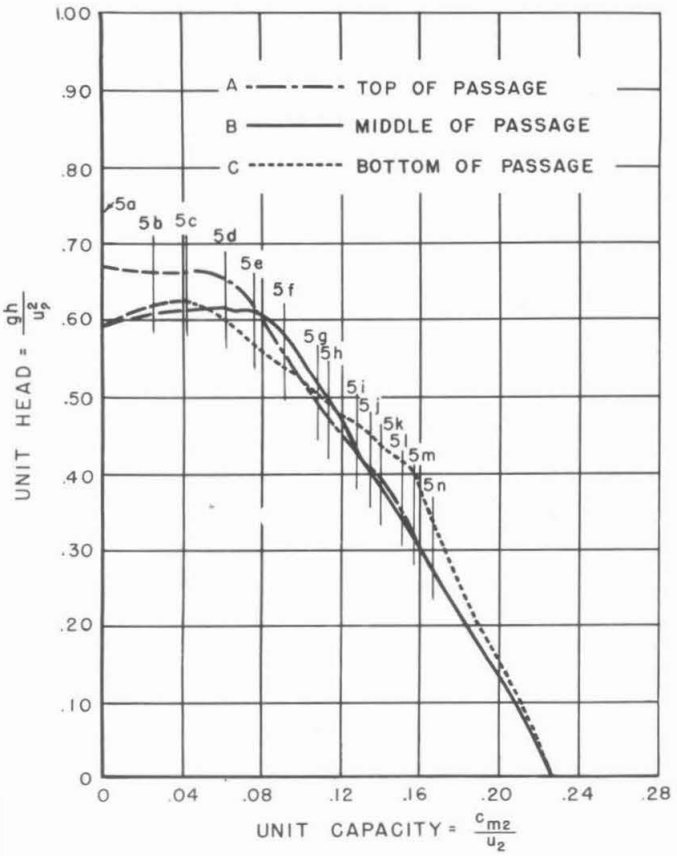

Fig. 6 - Unit head vs. unit capacity at three locations across the outlet width.

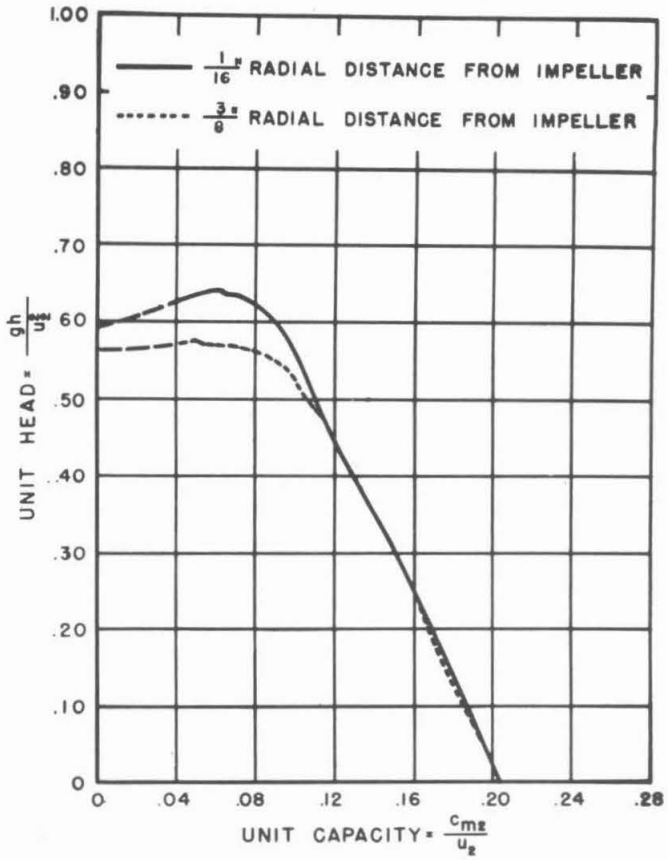

Fig. 7 - Effect of radial distance of total-head tube on measured head.

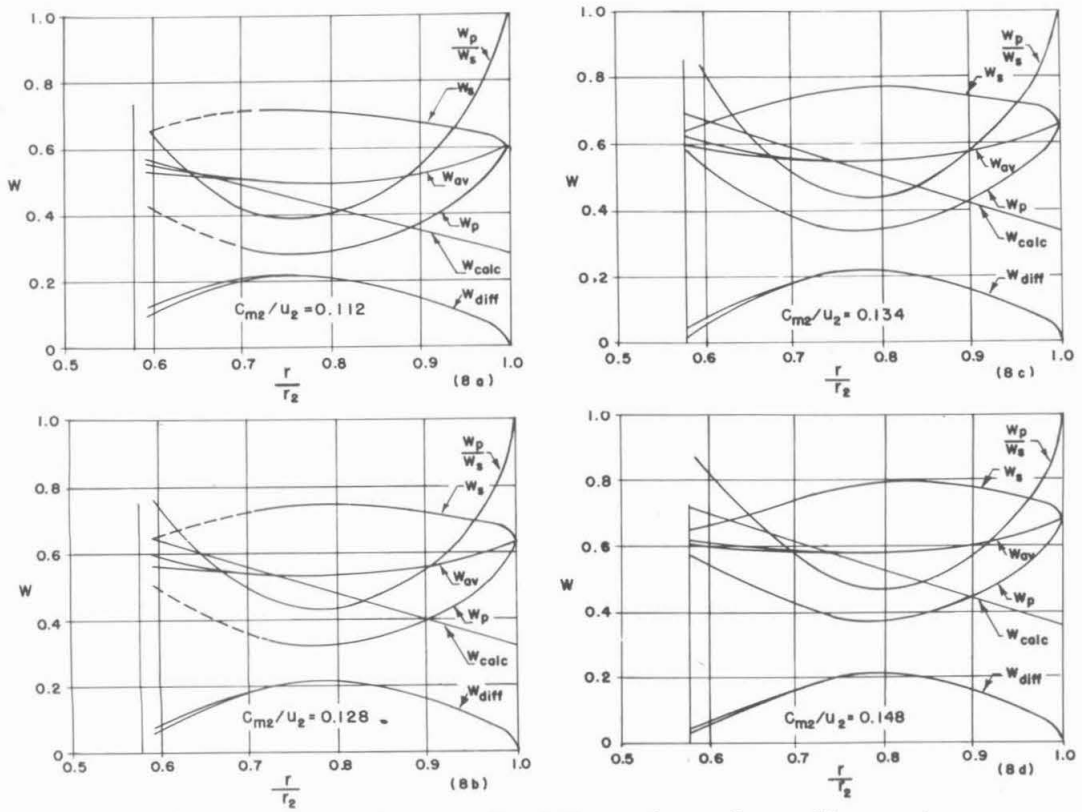

Fig. 8 - Dimensionless velocities at various flow rates.